ESI: Three-dimensional Heating and Patterning Dynamics of Particles in Microscale Acoustic Tweezers

Robert Weser [a], Zhichao Deng [b], Vijay V. Kondalkar [a], Alexandre N. Darinskii [c], Christian Cierpka [b], Hagen Schmidt [a*], Jörg König [b*]

[a]Leibniz Institute for Solid State and Materials Research Dresden, SAWLab Saxony, Dresden, Germany
Email Address: h.schmidt@ifw-dresden.de

[b]Institute of Thermodynamics and Fluid Mechanics, Technische Universität Ilmenau, Ilmenau, Germany
Email Address: joerg.koenig@tu-ilmenau.de

[c]Institute of Crystallography FSRC "Crystallography and Photonics", Russian Academy of Sciences, Moscow, Russia

Electronic supporting information includes the following sections

- Timing sequence and image analysis of APTV and LLI measurement
- Frequency dependent electrical characterization of the SAW device
- Particle arrangement at the first particle level ($\overline{z}_\mathrm{p} = 5.2\,\mu\mathrm{m}$)
- Transient state: Supplementary results
- Confirmation of particle trapping in all nodal levels
- Material properties for glycerol-water mixture used

Other supporting information include the following

- Supplementary Movie S1

Timing sequence and image analysis of APTV and LLI measurement

To avoid a systematic uncertainty caused by the high-energy laser light, we applied an LED as light source for the luminescence excitation. The timing sequence for the APTV and LLI measurement is depicted in Fig. S1. The first frame of the double-frame image was recorded exactly during the illumination of the LED. Therefore, the duration of illumination is identical to the exposure time of the first frame t_1 which was found to be optimal at 800 µs. Then after a very short inter-frame gap of (90-120) ns, the second frame was taken recording the whole emission phase of the phosphorescent dye. The exposure time of the second frame t_2 as governed by the read out time of the first frame was around 10 ms. During measurement, double-frame images were captured with a frame rate of 10 Hz corresponding to a time interval between subsequent double-frame images of $t_{cap} = 100$ ms. In comparison to conventional approaches [1,2], the timing strategy differs regarding the duration of the exposure times t_1 and t_2 as well as the timing of illumination, which takes place not before but at the same time as the exposure of the first frame. These adaptations compensated for the much lower illumination intensity of the LED and ensured a sufficient signal-to-noise ratio of the particle images for image analysis. However, the image processing approaches of the APTV and LLI analysis were identical to conventional methods [1,3].

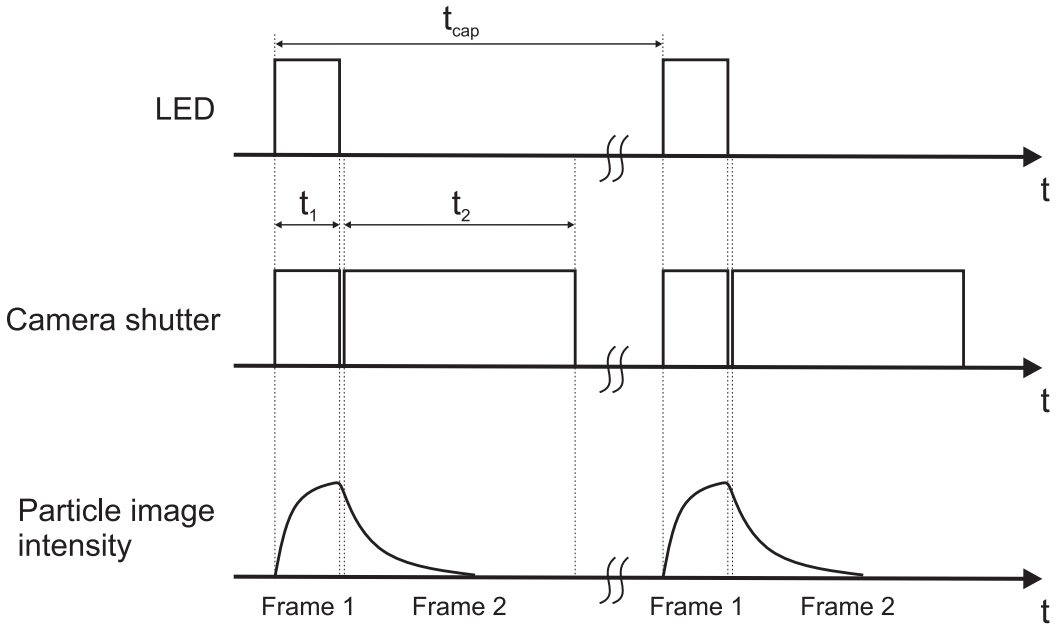

Fig. S1. Timing schedule for the APTV and LLI measurement.

Frequency dependent electrical characterization of the SAW device

Electrical characterization of SAW device was performed with a vector network analyzer yielding complex S-parameters. The reflection coefficient for a single IDT provides information on SAW excitation and indicates relevant electro-acoustic energy conversion in the frequency range 30.5 MHz to 34.5 MHz (Fig. S2a), in which the bandwidth for propagation in the $X+90^\circ$ direction on the 128° rotated Y-cut surface is lower as compared to the X direction due to the different number of IDT electrodes for both directions. The period of IDTs in both directions was adapted to enable SAW excitation at a common frequency (32.4 MHz). The transmission coefficient was measured for two opposing IDTs and both directions (Fig. S2b), furthermore providing information on SAW propagation between both IDTs. Transmission coefficients were measured for the three cases: bare substrate surface, the PDMS chamber attached to the surface, and the fluid-filled chamber. The relative differences of transmission were evaluated to estimate acoustic energy transfer from the SAW to the microfluidic structure.

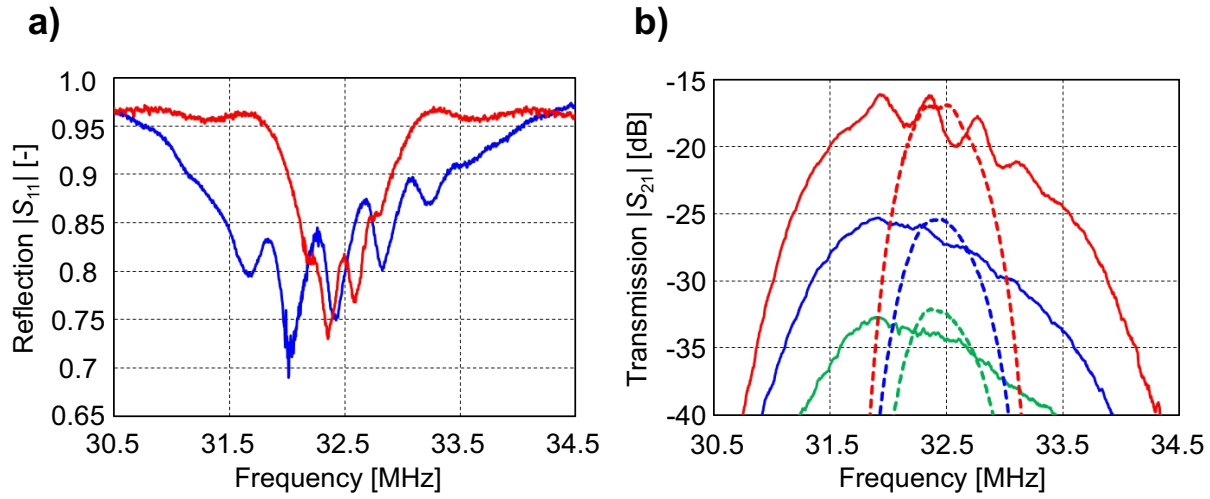

Fig. S2. Frequency dependent electrical characteristics of IDT arrangement. **a)** Reflection coefficient $|S_{11}|$ of single IDT in X direction (blue) and $X+90^\circ$ direction (red). The crystallographic axes X and $X+90^\circ$ correspond to the y- and x-direction of the setup, respectively. **b)** Transmission coefficient $|S_{21}|$ for opposing IDTs for bare substrate surface (red lines), PDMS chamber attached to the substrate surface (blue lines), and fluid-filled chamber (green lines). Transmission coefficients are given for IDTs in X direction (solid lines) and $X+90^\circ$ direction (dashed lines) coinciding with the y- and x-ordinate of the acoustofluidic setup, respectively.

Particle arrangement at the first particle level ($\bar{z}_\mathbf{p} = 5.2\,\mu\mathbf{m}$)

Particles arranged at the first particle level ($\bar{z}_\mathrm{p} = 5.2\,\mu\mathrm{m}$) were vertically arranged next to the substrate surface by the downwards directed ARF component (cf. Fig. 3c). The lateral particle pattern together with the distribution of ARF is given in Fig. S3. Particles are located at positions in between two neighboring maxima, like at the second particle level (cf. Fig. 4).

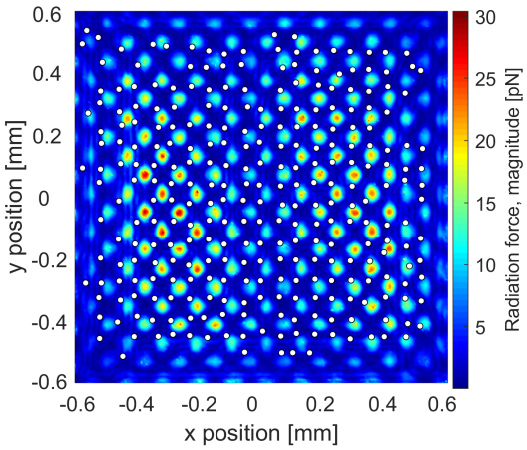

Fig. S3 Lateral particle pattern at the first particle level ($\bar{z}_\mathrm{p}$ =5.2 µm) induced by the steady-state acoustic field. Particle positions ($\bar{x}_\mathrm{p}$,$\bar{y}_\mathrm{p}$) are plotted over the lateral distribution of the according acoustic radiation force (magnitude, calculated with material properties for 50°C).

Transient state: Supplementary results

As it is shown for steady-state conditions, particles were trapped in two particle position levels, because of the sedimentation of particles at the substrate surface before SAW excitation. The first particle position level was found to be in close vicinity to the substrate surface whereas the second particle position level was found at a height corresponding to the first nodal level. The same behavior was observed during transient state measurements, independent of the acoustic power applied. Similar to the result at steady-state, more than 87% of the sedimented particles were trapped in the first particle position level. With time-resolved measurement of the z position of the particles during start-up phase of particle trapping (cf. Fig. 7a), the distance between particle and substrate surface was evaluated for all particles trapped within the first particle level. The result is given in the histogram depicted in Fig. S4. The mean height of the particles trapped in the first particle position level was determined to be 0.6 µm from the fitted normalized probability density function.
Furthermore, the mean particle trapping time of about 1.2 s was determined over all experimental runs and all acoustic power levels applied. According to the result depicted in Fig. S5, the measurements indicate a trend to shorter trapping times with increasing power levels. However, as the particle concentration was low, and the trapping depends not only on the acoustic power level but also on the position of the particles relative to the pressure minima, the variation of the trapping time was comparably high between the individual experimental runs. The error bars in Fig. S5 indicate this variation, representing the minimum and maximum trapping time determined for each acoustic power level.

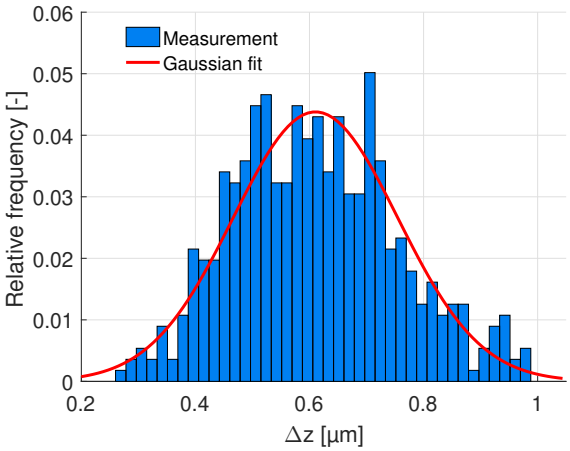

Fig. S4. Probability distribution of the elevation of the particles at the first particle position level. Measurements performed during transient state.

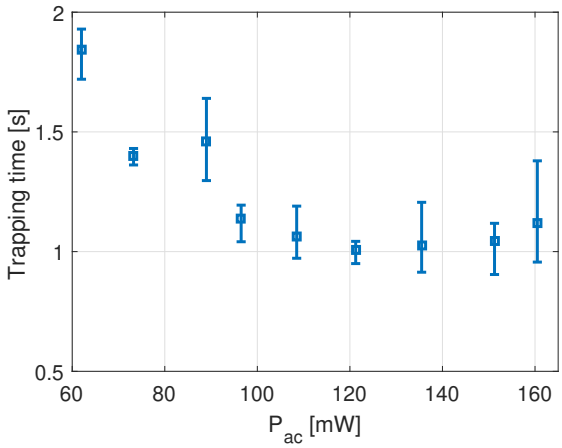

Fig. S5. Mean particle trapping time during the transient state. The error bars indicate the minimum and maximum trapping time.

Confirmation of particle trapping in all nodal levels

According to the measurement procedure described in the manuscript, particles were sedimented at the substrate surface before each measurement run. Due to this, particles were found only in direct vicinity to the substrate surface ($\bar{z}_\mathrm{p} = 5.2\,\mu\mathrm{m}$) and at the first nodal level ($z = 26\,\mu\mathrm{m}$) when the SAW was excited. In order to prove experimentally the existence of the second nodal level ($z = 58\,\mu\mathrm{m}$) and to confirm the numerical result, another series of 30 measurements with altered initial conditions has been conducted. Duration of the measurements, traversing of the measurement volume through the chamber as well as evaluation of the image captures were adopted from the measurement procedure described in subsection 2.4.2 of the manuscript. However, for these additional measurements, recording started immediately after introducing the particle suspension. Therefore, particles were still floating in the fluid when the SAW tweezer was switched on. With this procedure, particles were patterned in three particle levels, see Fig. S6. The third particle level with a mean particle position of ($\bar{z}_\mathrm{p} = 58.6\,\mu\mathrm{m}$) agrees well with the expected second nodal level and confirms the numerical result, compare also Fig. 3c in the manuscript.

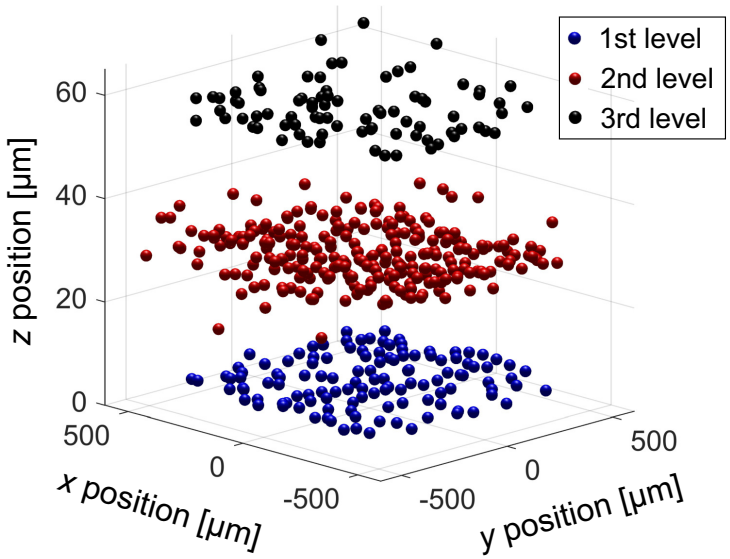

Fig. S6. Three-dimensional particle distribution inside the microfluidic chamber measured with immediate start of the experiment after (re-)filling the chamber with particle suspension. Under this initial condition, particles were found to be trapped at all three possible levels; close to the substrate surface (1st particle level) as well as at the first and at the second nodal level (i.e. at the 2nd and at the 3rd particle level).

Material properties for glycerol-water mixture

Temperature	40 °C	50 °C	60 °C
Density[4,5]	1144 $\mathrm{kg\,m^{-3}}$	1138.6 $\mathrm{kg\,m^{-3}}$	1133 $\mathrm{kg\,m^{-3}}$
Viscosity[4,5]	0.0052983 $\mathrm{N\,s\,m^{-2}}$	0.0038818 $\mathrm{N\,s\,m^{-2}}$	0.0029531 $\mathrm{N\,s\,m^{-2}}$
Sound velocity[6,7]	1774 $\mathrm{m\,s^{-1}}$	1765 $\mathrm{m\,s^{-1}}$	1751 $\mathrm{m\,s^{-1}}$

Table S1. Material properties for 55% glycerol-water mixture at different temperatures.

References

[1] J. Massing, C. J. Kähler and C. Cierpka, *Experiments in Fluids*, 2018, **59**, 163.

[2] C. Abram, I. W. Panjikkaran, S. N. Ogugua and B. Fond, *Optics Letters*, 2020, **45**, 3893–3896.

[3] C. Cierpka, M. Rossi, R. Segura and C. J. Kähler, *Measurement Science and Technology*, 2010, **22**, 015401.

[4] N.-S. Cheng, *Industrial and Engineering Chemistry Research*, 2008, **47**, 3285–3288.

[5] A. Volk and C. J. Kähler, *Experiments in Fluids*, 2018, **59**, 75.

[6] L. Negadi, B. Feddal-Benabed, I. Bahadur, J. Saab, M. Zaoui-Djelloul-Daouadji, D. Ramjugernath and A. Negadi, *The Journal of Chemical Thermodynamics*, 2017, **109**, 124–136.

[7] A. P. V. Egas, N. M. C. Talavera-Prieto, A. G. M. Ferreira, J. B. Santos, M. J. Santos, Z. L. Almeida and I. M. A. Fonseca, *The Journal of Chemical Thermodynamics*, 2021, **156**, 106367.